Spectral shape and broadening of emission from AlGaInP light-emitting diodes

N. C. Chen, W. C. Lien, Y. K. Yang, C. Shen, Y. S. Wang, and J. F. Chen

Citation: Journal of Applied Physics **106**, 074514 (2009); doi: 10.1063/1.3243319
View online: http://dx.doi.org/10.1063/1.3243319
View Table of Contents: http://scitation.aip.org/content/aip/journal/jap/106/7?ver=pdfcov
Published by the AIP Publishing

Spectral shape and broadening of emission from AlGaInP light-emitting diodes

N. C. Chen,[1,a)] W. C. Lien,[1] Y. K. Yang,[1] C. Shen,[1] Y. S. Wang,[2] and J. F. Chen[2]
[1]*Department of Electronic Engineering, Institute of Electro-Optical Engineering, Chang Gung University, Tao-Yuan, Taiwan 333, Republic of China*
[2]*Department of Electrophysics, National Chaio Tung University, Hsinchu, Taiwan 300, Republic of China*

(Received 3 July 2009; accepted 8 September 2009; published online 14 October 2009)

This work presents a model for describing the shape of the spontaneous emission spectrum from a quantum-well structure. A function is introduced to specify the probability distribution for the effective band gap. Based on this model, the coexisting carrier thermal broadening and effective band gap broadening in the spontaneous emission spectrum can be separated from each other. Applying this model to the spectra of AlGaInP light-emitting diodes reveals that the probability distribution functions are almost Gaussian. Therefore, the emission spectra can be described by an analytical expression with fitted parameters. Possible reasons for this band gap broadening are discussed. The determination of the junction temperatures from the emission spectra and possible deviations of the results thus determined are also elaborated. © *2009 American Institute of Physics*. [doi:10.1063/1.3243319]

I. INTRODUCTION

AlGaInP alloys are extremely important in visible light-emitting diodes (LEDs) with a yellow-green to red spectral range, because of their direct band gap, their lattice matching to the GaAs substrate, and the large range of tunability of their wavelengths.[1–3] Therefore, considerable effort has been made to enhance the performance of AlGaInP LEDs, including both the internal quantum efficiency[4–6] and the extraction efficiency.[7–14] Hence, current AlGaInP LEDs exhibit a luminous efficiency of as high as 100 lm/W,[14] and have already been adopted in numerous applications. However, in the light of rapid advances in device performance, there are a few studies on the fundamental properties of LED emission, such as spectral width and shape. The emission is generated by electron-hole recombination in the active layer, so the spectrum should depend strongly on numerous parameters, such as the energy distribution of carriers, the density of states, temperature, the coupling strength between electrons and holes, compositional fluctuations, and dimensional fluctuations. All of these important parameters can be investigated using the emission spectrum. For example, comparing the surface and edge emissions from AlGaInP LEDs reveals not only the origin of their difference, but also the electron-hole radiative recombination lifetime, the optical joint density of states, the absorption spectrum, and the bimolecular recombination coefficient of the quantum wells.[15]

This work presents a model for describing the shape of the spontaneous emission spectrum from a quantum-well structure. A function is introduced to specify the probability distribution for the effective band gap. Based on this model, the coexisting carrier thermal broadening and effective band gap broadening in the spontaneous emission spectrum can be separated from each other. Applying this model to the spectra of AlGaInP LEDs reveals that the probability distribution functions are almost Gaussian. Therefore, the emission spectra can be described by an analytical expression with fitted parameters. Possible reasons for this band gap broadening are discussed. The determination of the junction temperatures from the emission spectra, and possible deviations of the determined results from actual values are also considered.

II. EXPERIMENT

The spectra of two AlGaInP LEDs that separately emit yellow-green and amber were analyzed. The wafer structure of the yellow-green sample has an *n*-type GaAs substrate, a 390-nm-thick *n*-type $Al_{0.5}In_{0.5}P$ hole-blocking layer, 65 pairs of multiple quantum wells (MQWs), each of which comprises a 3.3 nm $(Al_{0.3}Ga_{0.7})_{0.5}In_{0.5}P$ well/2.9 nm $(Al_{0.58}Ga_{0.42})_{0.5}In_{0.5}P$ barrier, a 517-nm-thick *p*-type $Al_{0.5}In_{0.5}P$ electron-blocking layer, and a 9.38-μm-thick *p*-type GaP current spreading layer. Since the spectral characteristics of the amber sample are similar to those of the yellow-green sample, details of the wafer structure of the amber device are not elaborated here. Chips made from these wafers had an area of 225×225 μm^2 and a height of 180 μm. These chips were mounted onto heat sinks using a metal solder. The heat sink was a Bergquist thermal clad substrate with an area of 3×3 cm^2 and a height of 0.2 cm. According to the authors' earlier work, the thermal resistance of a device that is mounted in this method is less than 105 K/W.[16,17] Therefore, the junction temperature was less than 2.5 K greater the ambient temperature when the device was operated at 10 mA. The device spectra were obtained by placing the device onto the sample holder of a cryostat, electrically driving the device, collecting the top emission using a microscope, and then analyzing the wavelength-dependent energy spectral density functions $P(\lambda)$ using a monochromator and a silicon photodetector. The overall system wavelength-dependent response comprised of the responsiv-

[a)]Electronic mail: ncchen001@mail.cgu.edu.tw.

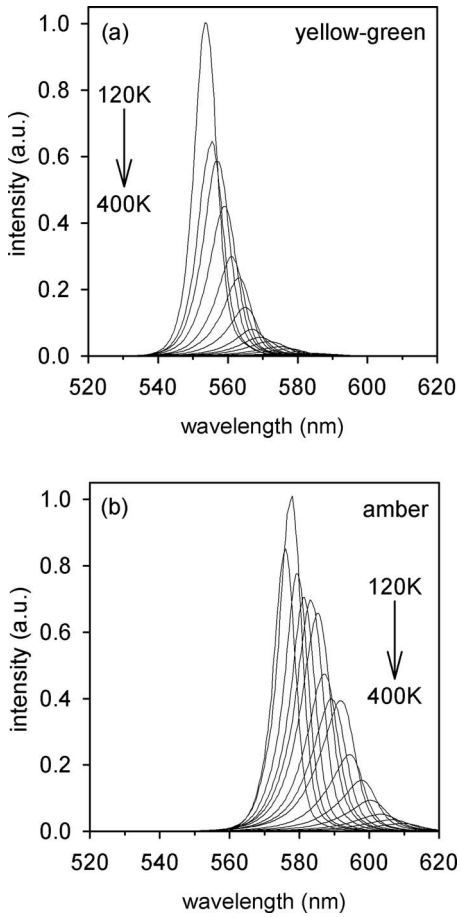

FIG. 1. Power spectra of (a) yellow-green and (b) amber LEDs measured at 10 mA. From bottom to top, ambient temperatures are from 400 to 120 K in steps of 20 K.

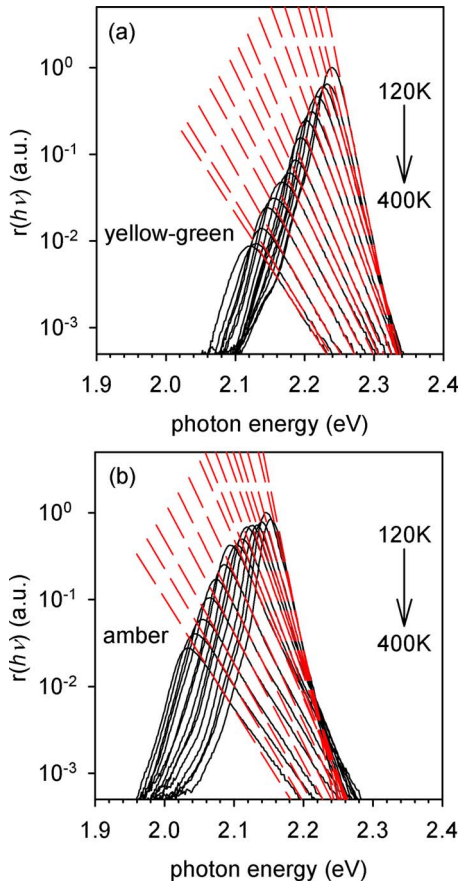

FIG. 3. (Color online) Photon density spectra of (a) yellow-green and (b) amber LEDs measured at 10 mA on a semi-log scale. From bottom to top, the ambient temperatures are from 400 to 120 K in steps of 20 K. The high-energy tails are accurately fitted by dashed straight lines with gradients $h\nu/KT$.

ity of the silicon photodetector and the reflectivity of the grating was taken into account. Figures 1(a) and 1(b) present the spectra of the yellow-green and the amber devices that were operated at 10 mA, at temperatures from 120 to 400 K in steps of 20 K, and the variations were summarized in Fig. 2. As the ambient temperature increased, the peaks were red-shifted and the intensities attenuated. As each photon represents a transition event in the active layer, the photon density spectrum is more useful than the power spectrum in obtaining information about spontaneous emission and the related phenomena. $P(\lambda)$ was then transformed to the corresponding frequency-dependent energy spectra $P(h\nu)$, according to $P(h\nu)=(\lambda^2/hC_0)P(\lambda)$, where C_0 is the speed of light in a vacuum and h is Planck's constant.[18] The relative photon density spectra $r(h\nu)$ were then obtained using $r(h\nu)=P(h\nu)/h\nu$,[15] and the results are plotted as solid curves on a semilog scale in Figs. 3(a) and 3(b) for the yellow-green and the amber devices, respectively.

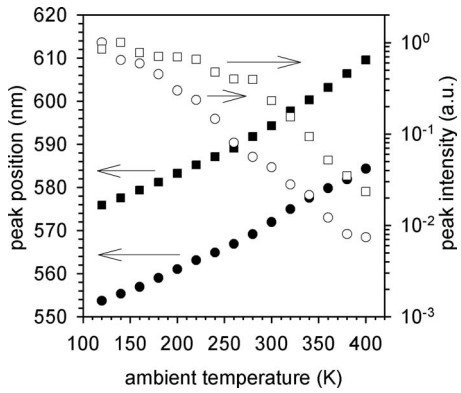

FIG. 2. Peak positions and peak intensities for yellow-green (circles) and amber (squares) devices, obtained from Fig. 1.

III. THEORETICAL SPECTRAL SHAPE

The spontaneous emission rate for a direct band gap semiconductor is[15,19]

$$r(h\nu) = \frac{1}{\tau_r}\rho(h\nu)f_c(1-f_v), \tag{1}$$

where τ_r is the electron-hole radiative recombination lifetime, $\rho(h\nu)$ is the optical joint density of states, and $f_c(1-f_v)$ is the probability that an electron is in the initial state and a hole is in the final state.[20] Since LEDs function with low-level excitation, $f_c(1-f_v)\approx e^{(E_{fn}-E_{fp})/KT}e^{-h\nu/KT}$, where $E_{fn}-E_{fp}$ is the separation between the quasi-Fermi energies of the electron and the hole.[21,22] Equation (1) becomes

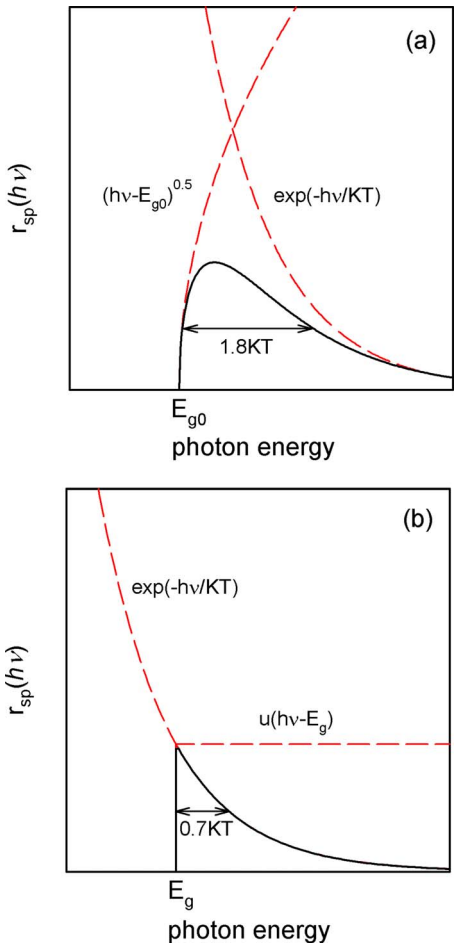

FIG. 4. (Color online) (a) Theoretical spontaneous emission spectra of (a) bulk material and of (b) quantum well. The dashed lines represent optical joint density of states and high-energy attenuation functions.

$$r(h\nu) = \frac{1}{\tau_r}\rho(h\nu)e^{(E_{fn}-E_{fp})/KT}e^{-h\nu/KT}. \tag{2}$$

For a bulk material, the optical joint density of state is $\rho(h\nu)=(2m_r)^{1.5}\sqrt{h\nu-E_{g0}}/2\pi^2\hbar^3$, where E_{g0} and m_r denote the band gap energy and the reduced mass of the electron-hole pairs, respectively. Thus, the spectrum of spontaneous emission should look like the solid curve in Fig. 4(a), which reveals the well-known $1.8KT$ full width at half maximum (FWHM). Likewise, in a quantum-well structure, since the motions of electrons and holes are confined in two-dimensional wells, the densities of states of the carriers are step functions, and the corresponding optical joint density of states is also a step function $\rho(h\nu)=m_r u(h\nu-E_g)/\pi\hbar^2 d$, where $u(\ )$ denotes the step function, d is the thickness of the quantum well, and E_g is the effective band gap, which includes the quantum-confined zero-point energies of electrons and holes. The resulting theoretical spectrum should be similar to the solid curve in Fig. 4(b), which rises sharply when $h\nu>E_g$ and has a FWHM of $0.7KT$.

However, the real spectra in Fig. 3 did not rise sharply when $h\nu>E_g$ and the corresponding FWHMs in Fig. 5 also greatly exceed the value predicted using Eq. (2). Linear regression yields approximate FWHMs of $18.6+1.11KT$ and $13.2+1.19KT$ in units of meV for yellow-green and amber

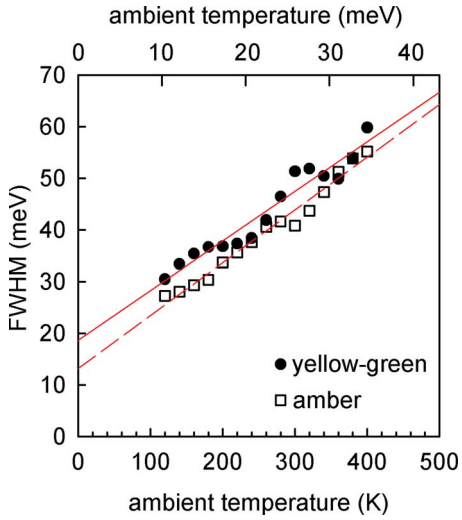

FIG. 5. (Color online) FWHM of photon density spectra in Fig. 3. The solid and dashed lines represent corresponding linear regressions.

devices, respectively. The fact that the FWHMs exceed 13 meV even when the temperature is extrapolated to 0 K indicates that the band gaps of the quantum wells are broadened. This broadening has many potential causes, including fluctuation of well width,[23–25] compositional fluctuation,[26] the low-energy tail of the band gap states,[21] and variations among wells. However, regardless of the actual reasons, a satisfactory analytical description of the experimental results must include the effects of the broadening. Therefore, a distribution function, $W(E_g)$, which satisfies the normalization condition

$$\int_0^\infty W(E_g)dE_g = 1, \tag{3}$$

is adopted herein to specify the probability distribution for the effective band gap. Because of this distribution, the collection of all the emissions from various band gaps constitutes the observed spectrum. Therefore, the spontaneous emission spectrum should be

$$\begin{aligned} r(h\nu) &= \int_0^\infty r(h\nu,E_g)W(E_g)dE_g \\ &= \frac{m_r}{\pi\hbar^2 d\tau_r}e^{(E_{fn}-E_{fp})/KT}e^{-h\nu/KT} \\ &\quad\times\int_0^\infty u(h\nu-E_g)W(E_g)dE_g \\ &= \frac{m_r}{\pi\hbar^2 d\tau_r}e^{(E_{fn}-E_{fp})/KT}e^{-h\nu/KT}\int_0^{h\nu} W(E_g)dE_g. \end{aligned} \tag{4}$$

This equation is somewhat more complex than that for the unbroadened spectrum. However, when $h\nu$ is much larger than the major distribution range of $W(h\nu)$, $W(h\nu)\approx 0$, $\int_0^{h\nu}W(E_g)dE_g \approx \int_0^\infty W(E_g)dE_g = 1$, and Eq. (4) can be approximated as

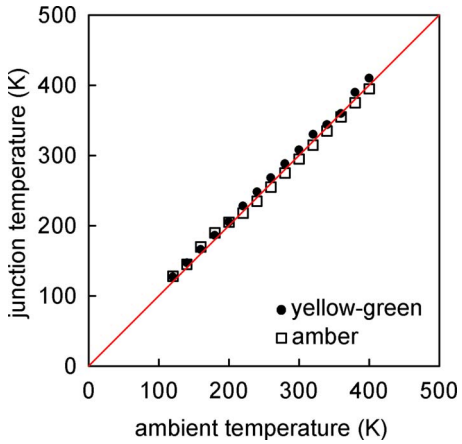

FIG. 6. (Color online) Dependences of junction temperatures on ambient temperatures obtained from gradients of high-energy tails in Fig. 3.

$$r(h\nu) \approx \frac{m_r}{\pi\hbar^2 d\tau_r} e^{(E_{fn}-E_{fp})/KT} e^{-h\nu/KT}. \tag{5}$$

This spectral shape is the same as that of the unbroadened spectrum [Eq. (2)] that attenuates as a function of $e^{-h\nu/KT}$ at the high-energy tail. This attenuation can be used as a metric of the temperature of the junction. Furthermore, since

$$r(h\nu)e^{h\nu/KT} = \frac{m_r}{\pi\hbar^2 d\tau_r} e^{(E_{fn}-E_{fp})/KT} \int_0^{h\nu} W(E_g)dE_g$$

$$\propto \int_0^{h\nu} W(E_g)dE_g, \tag{6}$$

the derivative of this equation with respect to $h\nu$ yields the shape of $W(h\nu)$ as follows:

$$W(h\nu) \propto \frac{\partial r[(h\nu)e^{h\nu/KT}]}{\partial(h\nu)}. \tag{7}$$

This proportionality in conjunction with the normalization condition, Eq. (3), exactly determines the band gap probability distribution function $W(h\nu)$.

IV. EXPERIMENTAL SPECTRAL ANALYSIS

As indicated by the solid curves in Figs. 3(a) and 3(b), although the ambient temperature covers a rather wide range (from 120 to 400 K), the slopes of the low-energy tails of the measured spectra do not change appreciably with the temperature. This fact is consistent with Eq. (4), which states that the low-energy tails of these spectra depend strongly on the broadening of the band gap but weakly on the junction temperature. In contrast, as revealed by the dashed lines in Figs. 3(a) and 3(b), the high-energy tails of these spectra are accurately described by straight lines whose gradients depend strongly on the temperature. Figure 6 plots the junction temperatures obtained from the gradients, which are very close to the ambient temperatures. This finding agrees with Eq. (5): When $h\nu$ exceeds the major distribution range of $W(h\nu)$, the high-energy tails of the broadened spectra are similar to that of the unbroadened spectrum that attenuates as a function of $e^{-h\nu/KT}$.

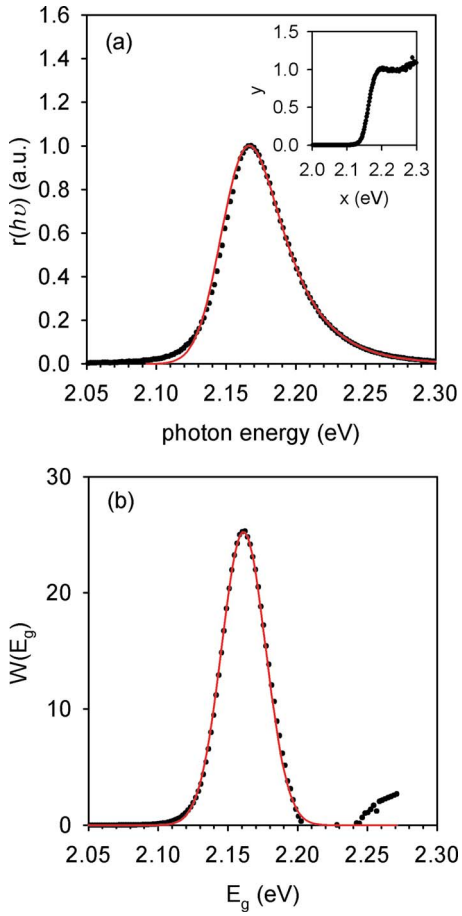

FIG. 7. (Color online) (a) Points plot spectrum of yellow-green sample measured at 300 K while solid curve plots simulated results. The inset plots the relationship between $\int_0^x W(E_g)dE_g$ and x obtained from measured spectrum. (b) Points plot effective band gap probability distribution function $W(E_g)$ obtained by differentiating the curve in inset in (a). These points are very close to a Gaussian distribution, plotted as a solid curve.

After the junction temperatures were determined, the band gap distribution functions $W(E_g)$ were determined from the spectra. Figure 7 presents an example of the determination of one such function. The solid points in Fig. 7(a) plot the spectrum obtained from the yellow-green sample at 300 K. The spectrum was multiplied by $e^{h\nu/KT}$, where T is the obtained junction temperature, and by a normalization constant to make the resultant function unity at high energy, yielding the integral $\int_0^x W(E_g)dE_g$ using Eq. (4), as plotted in the inset in Fig. 7(a). Differentiation with respect to x yielded $W(E_g)$, which is represented by the solid points in Fig. 7(b). Based on this procedure, $W(E_g)$ was obtained for the yellow-green and the amber devices at various temperatures and plotted as solid curves in Figs. 8(a) and 8(b), respectively. The temperature-induced band gap shrinkage caused the peaks of $W(E_g)$, presented in Fig. 9(a), to be redshifted as the temperature increased. The FWHMs of $W(E_g)$, presented in Fig. 9(b), can be approximated by linear regression as $25.7+0.27KT$ and $18.6+0.41KT$ in units of meV for the yellow-green and the amber devices, respectively. Table I summarizes the temperature dependences of the FWHMs. The temperature dependence of the FWHMs of $W(E_g)$ is much

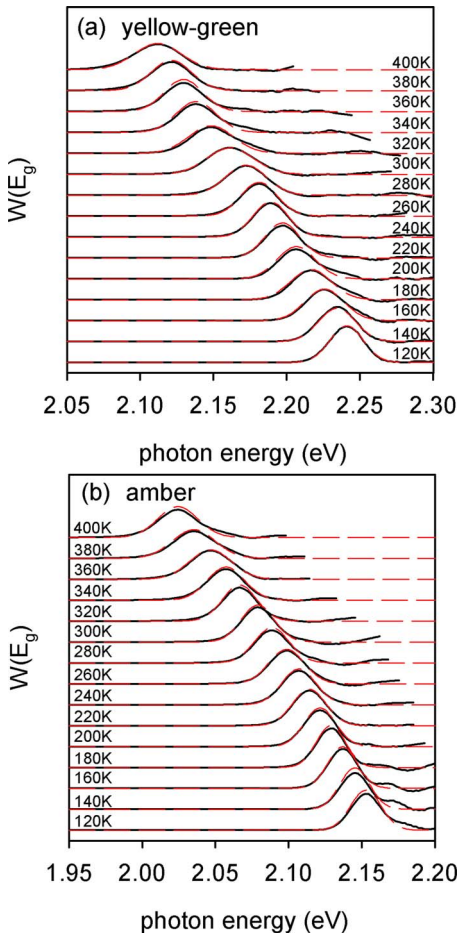

FIG. 8. (Color online) Solid curves plot effective band gap probability distribution functions obtained from Fig. 3, and dashed curves show corresponding Gaussian simulations.

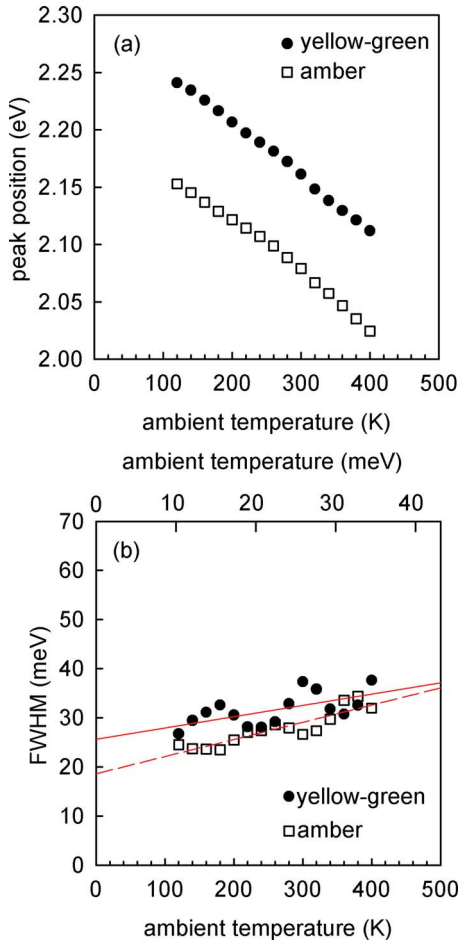

FIG. 9. (Color online) (a) Peak positions and (b) FWHM of effective band gap probability distribution functions in Fig. 8. The solid and dashed lines are corresponding linear regressions.

weaker than that of the original spectra, presented in Fig. 5 ($18.6+1.11KT$ and $13.2+1.19KT$), since broadening by thermal distribution of the carriers is eliminated.

Notably, all of the band gap distribution functions look like unit-area Gaussian functions

$$G(E_g - E_0, \Delta) = \frac{2}{\Delta}\sqrt{\frac{\ln 2}{\pi}} e^{-4\ln 2(E_g - E_0)^2/\Delta^2}, \tag{8}$$

where E_0 and Δ denote the central energy and the FWHM, respectively, of the distribution function, and E_g is the band gap parameter. For example, the band gap distribution function of the yellow-green sample, plotted in Fig. 7(b), is centered at E_0=2.161 eV and has a FWHM of Δ=0.037 eV. Substituting these E_0 and Δ values into the Gaussian function yields the solid curve in Fig. 7(b), which is markedly consistent with the experimentally determined band gap distribution function, except at the wings, where its intensity is low. This is not a special case since all of the experimentally determined band gap distribution functions in Fig. 8 (solid curves) can also be reasonably fitted by their corresponding Gaussian functions (dashed curves). Based on this observation, the theoretical spectrum that is given by Eq. (4) can be analytically expressed as

$$r_{sp}(h\nu) = \frac{m_r}{\pi\hbar^2 d\tau_r} e^{(E_{fn}-E_{fp})/KT} e^{-h\nu/KT} \times \begin{cases} \frac{1}{2}\mathrm{Erfc}\left(\frac{2\sqrt{\ln 2}|h\nu - E_0|}{\Delta}\right), & h\nu < E_0 \\ 1 - \frac{1}{2}\mathrm{Erfc}\left(\frac{2\sqrt{\ln 2}|h\nu - E_0|}{\Delta}\right), & h\nu \geq E_0, \end{cases} \tag{9}$$

where Erfc( ) is the complementary error function. The simulated spectrum of the yellow-green sample at 300 K, plotted as the solid curve in Fig. 7(a), is very close to the experimental solid points. This closeness is also evident in Fig. 10. All of the experimental spectra that were investigated in this work are represented as solid curves, while the corresponding simulated spectra are plotted as dashed curves. Accord-

TABLE I. Linear regression of FWHMs of photon density spectra in Fig. 3, and of effective band gap probability distribution functions in Fig. 8. The units are meV.

Sample	Yellow-green	Amber
Photon density spectra $r(h\nu)$	$18.6+1.11KT$	$13.2+1.19KT$
Band gap distribution function $W(E_g)$	$25.7+0.27KT$	$18.6+0.41KT$

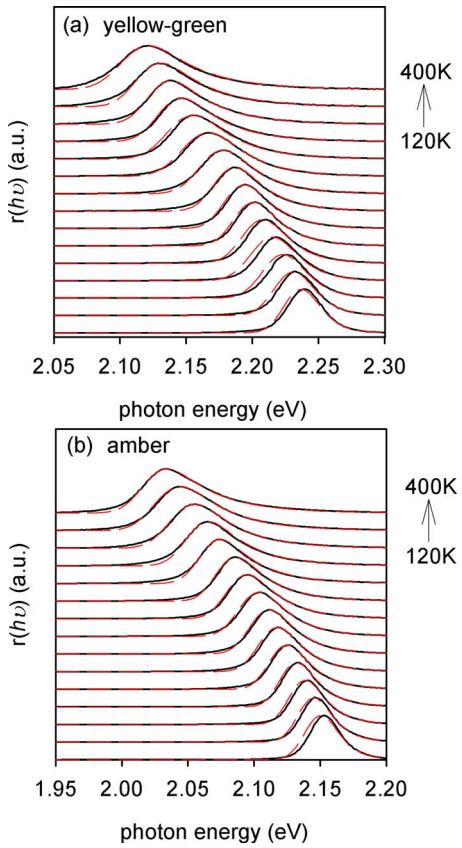

FIG. 10. (Color online) Measured (solid curves) and simulated (dashed curves) photon density spectra. From bottom to top, ambient temperatures are from 120 to 400 K in steps of 20 K.

ingly, Eq. (9) effectively simulates the spontaneous emission spectrum from a quantum-well structure.

V. DISCUSSION

The broadening of the high-energy tail of a spontaneous emission spectrum is caused mainly by the thermal distributions of the electrons and holes. Thus, the temperature obtained from the high-energy tail, or equivalently, determined from the equation

$$T = -\frac{1}{K}\left(\frac{\partial \ln[r(h\nu)]}{\partial(h\nu)}\right)^{-1}, \tag{10}$$

is frequently called the carrier temperature T_c, in contrast to the junction temperature T_j, which specifically refers to the lattice temperature in this situation. In the cases considered herein, the measured carrier temperatures are close to the lattice temperatures. However, the authors' experience has also established that many other devices, especially nitride LEDs, have a higher carrier temperature, as indicated frequently in literature.[27–35] Henry *et al.*[36–38] addressed this issue by considering the balance of energy flow and concluded that the real carrier temperature should not deviate appreciably from the lattice temperature. Their argument, when applied to the cases in this work, is modified as follows. Since the room-temperature bimolecular recombination coefficient between the electrons and holes is $B=1.87\times10^{-10}$ cm^3 s^{-1} in the AlGaInP quantum wells herein,[15] when the devices are operated at $I=10$ mA and assumed to have a 100% internal quantum efficiency, the carrier injection rate, the injected excess carrier density, and the radiative excess carrier lifetime are $R_r=5.75\times10^{24}$ cm^{-3} s^{-1}, $\Delta n=1.75\times10^{17}$ cm^{-3}, and $\tau_c=30.5$ ns, respectively, derived from the equality $R_r=(I/e)/V=B\Delta n^2=\Delta n/\tau_c$, where V denotes the total volume of the quantum wells. Now, the energy relaxation time τ_E required to yield $T_c-T_j=10$ K can be estimated. The temperature difference between the carriers and the lattice causes the rate of energy loss from the electron-hole pairs to the lattice to be $3\Delta nk(T_c-T_j)/\tau_E$. However, since an electron-hole pair that moves from the barrier to the quantum well should obtain a kinetic energy $E_{\text{offset}}\approx0.1$ eV from the offset between the barriers and the zero-point energies in the wells, the carrier heating rate is $R_rE_{\text{offset}}=\Delta nE_{\text{offset}}/\tau_c$. Since both rates must be equal in the steady state, the energy relaxation time is estimated to be $\tau_E=3k(T_c-T_j)\tau_c/E_{\text{offset}}\approx788$ ps. This value is unreasonably large in comparison to 2.5 ps for n-type GaAs and 1.7 ps for n-type InP,[39] and is the result of overestimation of the temperature difference. Accordingly, a high carrier temperature, measured from the high-energy tail, does not really reflect the true carrier temperature; rather, it reflects the fact that the high-energy tail of the spectrum cannot be fully described by the attenuation factor $e^{-h\nu/KT}$.

The deviation of the high-energy tail from pure exponential decay has many potential causes. The first is the improper transformation of the measured spectrum. For example, if the spectral analyzer has been carefully calibrated and the measured result corresponds to the wavelength-dependent power spectrum, then not only should the x-axis be changed from wavelength to frequency, but also the y-axis, as stated above, should be changed to the frequency-dependent photon density. If the transformation of the y-axis is ignored, then, although the determined peak position of the spectrum will not be significantly affected, the shape of the spectrum will be changed, and the carrier temperature obtained from the improperly transformed spectrum will be $T_m=T_c/[1-3KT_c/h\nu]$, where T_m is the measured carrier temperature, T_c is the real carrier temperature, and $h\nu$ is the energy at which T_m is determined. Therefore, when $T_c=300$ K and $h\nu=2.2$ eV, the measured carrier temperature is $T_m=311$ K, which exceeds the real carrier temperature. The second possible cause is the deviation in the optical joint density of states. For example, in double heterostructure or homojunction LEDs, the optical joint density of states is proportional to $(h\nu-E_g)^{0.5}$, and the measured carrier temperature is $T_m=T_c/[1-KT_c/2(h\nu-E_{g0})]$. Thus, at $T_c=300$ K and $h\nu-E_{g0}=50$ meV, the measured carrier temperature is $T_m=405$ K, which markedly exceeds the real carrier temperature. The third possible cause is the broadening of the band gap.[31–35] For example, if this broadening follows a Gaussian function as in the cases presented herein, then the measured carrier temperature is

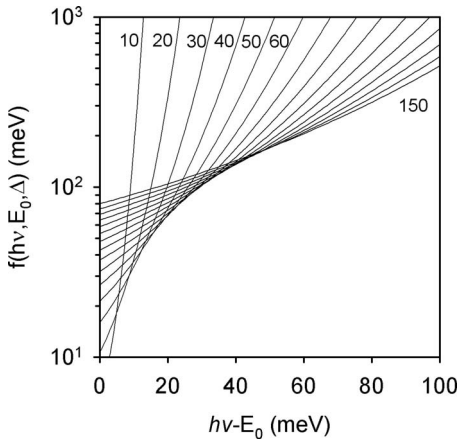

FIG. 11. Dependence of $f(h\upsilon, E_0, \Delta)$ on $h\upsilon - E_0$ and Δ. From left to right, Δ is from 10 to 150 meV in steps of 10 meV.

$$T_m = \frac{T_c}{1 - \dfrac{G(h\upsilon - E_0, \Delta)}{\displaystyle\int_0^{h\upsilon} G(x - E_0, \Delta)dx} KT_c}. \tag{11}$$

where $G(\ )$, E_0, and Δ are defined in Eq. (8). This equation can be further simplified to

$$\frac{T_m - T_c}{T_c} \approx \frac{KT_c}{f(h\upsilon, E_0, \Delta)}, \tag{12}$$

where $f(h\upsilon, E_0, \Delta) = \int_0^{h\upsilon} G(x - E_0, \Delta)dx / G(h\upsilon - E_0, \Delta)$, as plotted in Fig. 11 for various Δ and $h\upsilon - E_0$. Consider the yellow-green sample described above and presented in Fig. 7(b) as an example; since the broadening Δ is only 37 meV, $f(h\upsilon, E_0, \Delta)$ equals 6222 meV and markedly exceeds KT_c when $h\upsilon - E_{g0} = 50$ meV. Thus, the deviation of the measured carrier temperature T_m from the real carrier temperature T_c is only 0.4% when $T_c = 300$ K. Accordingly, the measured carrier temperatures were almost the same as the lattice temperatures. However, if Δ is extended to $5KT$, $f(h\upsilon, E_0, \Delta)$ equals 171 meV. The deviation of the measured carrier temperature T_m from the real carrier temperature T_c is 15%, and the measured carrier temperature should be 345 K, which greatly exceeds the real carrier temperature. The fourth possible cause is the reabsorption of the spontaneous emission by the quantum wells. By this reabsorption, the spontaneous emission spectrum $r(h\nu)$ should be attenuated to become $r(h\nu)[1 - \exp(-\alpha(h\nu)L)] / \alpha(h\nu)L$, where $\alpha(h\nu)$ is the absorption coefficient that can be deduced from $r(h\nu)$ via the relationship between Einstein's A and B coefficients, and L is the total thickness of the light-emitting layer.[15] The parameters $E_0 = 2.161$ eV, $\Delta = 0.037$ eV, and $T = 300$ K were substituted into Eq. (9), which describes the theoretical spontaneous emission spectrum, to determine the relation between the carrier temperatures measured at $h\upsilon - E_{g0} = 50$ meV and the number of quantum wells. The results plotted in Fig. 12 clearly show that the deviation between the measured and the real carrier temperatures is less than 7 K, even when the number of quantum wells reached an unreasonably large value of 1000. This small deviation is the result of the constant optical joint density of states that causes the absorption coefficient to depend weakly on the energy when $h\upsilon \gg E_{g0}$. Thus, the high-energy tail of the spectrum was attenuated by a similar factor at various energies, and the measured carrier temperature is always very close to the real carrier temperature. Therefore, reabsorption cannot be a major cause of largely responsible for the overestimation of carrier temperature in a two-dimensional structure.

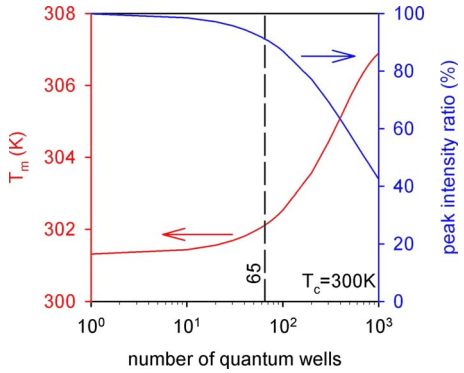

FIG. 12. (Color online) Effects of reabsorption on measured carrier temperature and peak intensity.

After the broadening effect, induced by the thermal distribution of carriers, has been eliminated from the spontaneous emission spectra, the resulting probability distributions of the effective band gap, presented in Figs. 7(b) and 8, still reveal significant line widths. Moreover, the widths of these distributions still depend weakly on the lattice temperature. Thus, the possible determinants of the line shape, the line width, and the temperature dependence of the width are of great interest. The Gaussian behavior of these distribution functions, according to the central limit theorem in statistics and probability theory, indicates that the broadening is probably related to some random distribution in the active layers. The random distribution in the structures has two possible causes. The first is fluctuation of and variation among the well widths.[23–25] If the standard deviation of the well thickness is assumed to be the thickness of a single monolayer, then solving Schrödinger's equation using the effective mass approximation yields a deviation of the ground state transition between the electrons and the holes of $\sigma = 6.24$ meV. Thus, the FWHM is $\Delta = 2\sqrt{\ln 2}\sigma = 14.7$ meV. This value is about half of the experimental broadening, presented in Fig. 9(b), and is evidence of the importance of the thickness fluctuation to band gap broadening. The second cause is alloy broadening,[32–35] which results from the statistical fluctuation of the random distribution of the cations in $(Al_xGa_{1-x})_yIn_{1-y}P$. The quantitative model that was proposed by Schubert and co-workers[2,40,41] and the parameters in literature yield a broadening of the electron (hole) level, due to fluctuation of the composition parameter x, of $3.62 \times 10^{-9}/\sqrt{V_e}$ meV cm$^{-3/2}$ $(7.98 \times 10^{-10}/\sqrt{V_h}$ meV cm$^{-3/2})$ and a broadening due to the fluctuation of y of $1.17 \times 10^{-8}/\sqrt{V_e}$ meV cm$^{-3/2}$ $(2.57 \times 10^{-9}/\sqrt{V_h}$ meV cm$^{-3/2})$, where $V_{e(h)}$ denotes the volume that is enclosed by the electron (hole) mean free path $\ell_{e(h)}$ and equals $\pi(\ell_{e(h)}/2)^2 d$ in the cases considered herein. Thus, the FWHM of the effective band gap distribution is $\Delta = (1.50 \times 10^{-16}/V_e + 7.26$

$\times 10^{-18}/V_h)^{1/2}$ meV $cm^{-3/2}$. The electron (hole) mean free path in a two-dimensional structure can be determined from the relation $\ell_{e(h)}=v_{th,e(h)}\tau_{e(h)}=\sqrt{2KT/m_{e(h)}\tau_{e(h)}}$, where $v_{th,e(h)}$ is the thermal velocity, $\tau_{e(h)}$ is the momentum relaxation time, and $m_{e(h)}$ is the effective mass of the electrons (holes). Given the typical value $\tau_{e(h)}\sim 10^{-13}$ s used in the estimation,[40] the mean free paths of the electrons and holes are 28 and 12 nm, respectively, and the FWHM associated with alloy broadening is 9.6 meV. This value is comparable to that ascribed to the well width fluctuation, and demonstrates the role of alloy broadening in the devices. Moreover, when the temperature is increased, the phonon population is also increased, the momentum relaxation time of carrier $\tau_{e(h)}$ is decreased, the coherent volume of the carrier wave function $V_{e(h)}$ is reduced, and the compositional fluctuation increases, since a smaller volume has fewer cation sites. These changes may explain why the line widths of the effective band gap distributions still depend weakly on the temperature, even when the thermal broadening effect of the carrier distribution has been removed.

VI. CONCLUSION

This work presents a model for describing the spectra of quantum wells. A function $W(E_g)$ is introduced to specify the probability distribution for the effective band gap. The shape of the spectrum is determined by the product of the integral of $W(E_g)$ and the high-energy attenuation function $e^{-h\nu/KT}$. Accordingly, the carrier temperature can be determined from the high-energy tail of the spectrum and the probability distribution function can be deduced by further numerical processing. This model was applied to AlGaInP LEDs, and the measured carrier temperatures were found to be very close to the set lattice temperatures. This finding is important evidence of the validity of the proposed model. Since the probability distribution functions of the samples were almost Gaussian functions, the experimental spectra can be directly described by an analytical expression with fitted parameters. Well width and composition fluctuations are presumed to be responsible for $W(E_g)$ broadening, as determined from their orders of magnitude. The inherent randomness of these two mechanisms explains the Gaussian nature of the distribution functions. In spite of the successful application of this model herein, an excess of the carrier temperature over the lattice temperature, determined from the high-energy tail, is also frequently encountered. In such cases, the measured carrier temperature may not reflect the true carrier temperature, but indicates that the high-energy tail deviates from pure exponential decay. Four possible causes of this deviation are discussed. They are improper transformation of the measured spectrum, samples having different optical joint densities of states with respect to a quantum-well structure, excessive broadening of the band gap distribution function, and reabsorption of the emission by the active layer. The last, however, has less effect than the others.

ACKNOWLEDGMENTS

The authors would like to thank the National Science Council of the Republic of China, Taiwan, for financially supporting this research. Ted Knoy is appreciated for his editorial assistance.

[1] D. P. Bour and J. R. Shealy, IEEE J. Quantum Electron. **24**, 1856 (1988).
[2] A. T. Meney, A. D. Prins, A. F. Philips, J. L. Sly, E. P. O'Reilly, D. J. Dunstan, and A. R. Adams, IEEE J. Sel. Top. Quantum Electron. **1**, 697 (1995).
[3] D. Patel, J. M. Pikal, C. S. Menoni, K. J. Thomas, F. A. Kish, and M. R. Hueschen, Appl. Phys. Lett. **75**, 3201 (1999).
[4] C. P. Kuo, R. M. Fletcher, T. D. Osentowski, M. C. Lardizabal, M. G. Craford, and V. M. Robbins, Appl. Phys. Lett. **57**, 2937 (1990).
[5] H. Sugawara, K. Itaya, M. Ishikawa, and G. Hatakoshi, Jpn. J. Appl. Phys., Part 1 **31**, 2446 (1992).
[6] N. F. Gardner, H. C. Chui, E. I. Chen, M. R. Krames, J. W. Huang, F. A. Kish, S. A. Stockman, C. P. Kocot, T. S. Tan, and N. Moll, Appl. Phys. Lett. **74**, 2230 (1999).
[7] H. Sugawara, M. Ishikawa, and G. Hatakoshi, Appl. Phys. Lett. **58**, 1010 (1991).
[8] H. Sugawara, K. Itaya, H. Nozaki, G. Nozaki, and G. Hatakoshi, Appl. Phys. Lett. **61**, 1775 (1992).
[9] K. H. Huang, J. G. Yu, C. P. Kuo, R. M. Fletcher, T. D. Osentowski, L. J. Stinson, M. G. Craford, and A. S. H. Liao, Appl. Phys. Lett. **61**, 1045 (1992).
[10] F. A. Kish, F. M. Steranka, D. C. DeFevere, D. A. Vanderwater, K. G. Park, C. P. Kuo, T. D. Osentowski, M. J. Peanasky, J. G. Yu, R. M. Fletcher, D. A. Steigerwald, M. G. Craford, and V. M. Robbins, Appl. Phys. Lett. **64**, 2839 (1994).
[11] F. A. Kish, D. A. DeFevere, D. A. Vanderwater, G. R. Trott, R. J. Weiss, and J. S. Major, Electron. Lett. **30**, 1790 (1994).
[12] R. H. Horng, D. S. Wuu, S. C. Wei, C. Y. Tseng, M. F. Huang, K. H. Chang, P. H. Liu, and K. C. Lin, Appl. Phys. Lett. **75**, 3054 (1999).
[13] P. H. Chang, N. C. Chen, Y. N. Wang, C. F. Shih, M. H. Wu, T. H. Yang, Y. H. Tzou, and S. J. Wang, J. Vac. Sci. Technol. B **23**, L22 (2005).
[14] M. R. Krames, M. Ochiai-Holcomb, G. E. Höfler, C. Carter-Coman, E. I. Chen, I. H. Tan, P. Grillot, N. F. Gardner, H. C. Chui, J. W. Huang, S. A. Stockman, F. A. Kish, M. G. Craford, T. S. Tan, C. P. Kocot, M. Hueschen, J. Posselt, B. Loh, G. Sasser, and D. Collins, Appl. Phys. Lett. **75**, 2365 (1999).
[15] N. C. Chen, C. M. Lin, C. Shen, W. C. Lien, and T. Y. Lin, Opt. Express **16**, 20759 (2008).
[16] N. C. Chen, Y. K. Yang, Y. N. Wang, and Y. C. Huang, Appl. Phys. Lett. **90**, 181104 (2007).
[17] N. C. Chen, C. M. Lin, Y. K. Yang, C. Shen, T. W. Wang, and M. C. Wu, Jpn. J. Appl. Phys. **47**, 8779 (2008).
[18] N. C. Chen, Y. N. Wang, C. Y. Tseng, and Y. K. Yang, Appl. Phys. Lett. **89**, 101114 (2006).
[19] B. E. A. Saleh and M. C. Teich, *Fundamentals of Photonics* (Wiley, New York, 1991), p. 583.
[20] H. D. Summers, J. D. Thomson, P. M. Smowton, P. Blood, and M. Hopkinson, Semicond. Sci. Technol. **16**, 140 (2001).
[21] P. Blood, E. D. Fletcher, P. J. Hulyer, and P. M. Smowton, Appl. Phys. Lett. **48**, 1111 (1986).
[22] P. Blood, A. I. Kucharska, J. P. Jacobs, and K. Griffiths, J. Appl. Phys. **70**, 1144 (1991).
[23] P. Zhou, H. X. Jiang, R. Bannwart, S. A. Solin, and G. Bai, Phys. Rev. B **40**, 11862 (1989).
[24] C. Weisbuch, R. Dingle, A. C. Gossard, and W. Wiegmann, Solid State Commun. **38**, 709 (1981).
[25] C. Weisbuch, R. Dingle, A. C. Gossard, and W. Wiegmann, J. Vac. Sci. Technol. **17**, 1128 (1980).
[26] J. J. Coleman, P. D. Dapkus, M. D. Camras, N. Holonyak, Jr., W. D. Laidig, T. S. Low, M. S. Burroughs, and K. Hess, J. Appl. Phys. **52**, 7291 (1981).
[27] J. Shah, R. F. Leheny, R. E. Nahory, and H. Temkin, Appl. Phys. Lett. **39**, 618 (1981).
[28] B. Etienne, J. Shah, R. F. Leheny, and R. E. Nahory, Appl. Phys. Lett. **41**, 1018 (1982).
[29] M. Yamanishi, I. Suemune, K. Nonomura, and N. Mikoshiba, Jpn. J. Appl. Phys., Part 2 **21**, L240 (1982).

[30]O. Wada, S. Ymakoshi, and T. Sakurai, Appl. Phys. Lett. **41**, 981 (1982).
[31]T. Gessmann, E. F. Schubert, J. W. Graff, and K. Streubel, Proc. SPIE **4996**, 26 (2003).
[32]S. Chhajed, Y. Xi, Y. L. Li, T. Gessmann, and E. F. Schubert, J. Appl. Phys. **97**, 054506 (2005).
[33]Y. Xi, J.-Q. Xi, T. Gessmann, J. M. Shah, J. K. Kim, E. F. Schubert, A. J. Fischer, M. H. Crawford, K. H. A. Bogart, and A. A. Allerman, Appl. Phys. Lett. **86**, 031907 (2005).
[34]Y. Xi, T. Gessmann, J. Xi, J. K. Kim, J. M. Shah, E. F. Schubert, A. J. Fischer, M. H. Crawford, K. H. A. Bogart, and A. A. Allerman, Jpn. J. Appl. Phys., Part 1 **44**, 7260 (2005).
[35]P. Manninen and P. Orreveteläinen, Appl. Phys. Lett. **91**, 181121 (2007).
[36]C. H. Henry, R. A. Logan, H. Temkin, and F. R. Merritt, IEEE J. Quantum Electron. **19**, 941 (1983).
[37]C. H. Henry, R. A. Logan, and F. R. Merritt, J. Appl. Phys. **51**, 3042 (1980).
[38]C. H. Henry, R. A. Logan, and K. A. Bertness, J. Appl. Phys. **52**, 4453 (1981).
[39]G. H. Glover, Appl. Phys. Lett. **21**, 409 (1972).
[40]E. F. Schubert, E. O. Göbel, Y. Horikoshi, K. Ploog, and H. J. Queisser, Phys. Rev. B **30**, 813 (1984).
[41]E. F. Schubert, *Light-Emitting Diodes* (Cambridge University Press, Cambridge, 2003), p. 165.